OPTICAL AND LUMINESCENCE PROPERTIES OF

ERBIUM, YTTERBIUM, AND TERBIUM DOPED IN

ALUMINUM NITRIDE

THESIS SUBMITTED FOR THE DEGREE

MASTER OF SCIENCE

BY

TYLER R. CORN

ADVISOR

DR. MUHAMMED MAQBOOL

DEPARTMENT OF PHYSICS AND ASTRONOMY

BALL STATE UNIVERSITY

MUNCIE, INDIANA

JUNE 2010

ACKNOWLEDGEMENTS

Many thanks are given to my mother whom I owe so much. If not for her, school would not have been possible and my education would have been nonexistent. There are not enough good things I can say about how much I have been supported by her emotionally and financially. With her, all this was possible.

In combination with my mother, many other family members need to be mentioned as they have given me countless hours of support. My sister, father, and nana are some of my biggest fans for me completing a Master's in Physics. I hope I've made them proud!

Along with that, numerous friends I've made along the way that have guided me through all of my endeavors throughout the past years. The time has finally come to where I can say I am truly grateful for all that you've done for me, all the time we've spent together, and all the time that is destined to come. It may be a small town, but I couldn't have found friends like you anywhere else.

Lastly, my advisor and all the professors I've had during my time here at Ball State University. Without you, this wouldn't have even been an option! It takes dedicated and inspired people to do what you all do and inspire students, and for that, I thank you. A special thanks to my advisor for helping me along the way!

Table of Contents

List of Figures

List of Tables

Chapter 1

1.1   Introduction

In recent years, great interest has been focused on rare-earth elements doped into nitride semiconductors for their potential applications in the biomedical field as well as device fabrication, display technologies, and lasing properties [1 - 4]. Each of these applications requires the study of certain rare-earth elements' properties to further research into their respective field. Properties such as high thermal conductivity, stability, and optical/luminescence of nitride semiconductors make them very useful in furthering today's research and understanding. Electrical, optical, photonic and thermal uses were deduced from research with each rare-earth element. Increased interest has also grown from the idea of thermal quenching decreasing with increasing bandgap for a given nitride semiconductor. Hence, aluminum nitride has been chosen given its wide bandgap and unknown interaction with certain rare earth elements [6 - 12].

When a rare-earth element is doped into a semiconductor, sharp line emission was produced through excitation by different means. These emissions occur from the excitation and de-excitation of shell transitions within each rare-earth atom [13, 14]. Rare-earth elements studied here include erbium, terbium, and ytterbium. Photoluminescence was performed for each material as well as the combination of erbium and ytterbium. Photoluminescence is the process by which a material is

bombarded with photons, becomes excited, and then emits photons back into the system from the given material. In this research, rare-earth elements are being excited by photons from a laser and their de-excitation is recorded from the photomultiplier tube inside the spectrometer. Rare-earth elements are studied by doping them onto a thin film nitride semiconductor. Four of the most common nitride semiconductors are aluminum nitride, boron nitride, gallium nitride, and indium nitride. Aluminum was chosen as the best choice due to its bandgap (detailed in later chapters) [6 – 12]. Comparison of erbium and ytterbium was made from photoluminescence spectra using a 532 nm green laser and a 783 nm infrared laser. The combination of erbium and ytterbium in the same semiconductor also gives rise to new properties in terms of how each element reacts with others. Energy levels of these rare-earth elements are known [15, 16]; however, research will be focused around detectable energy level transitions and mainly the interaction between erbium and ytterbium by photoluminescence.

Rare-earth elements are chosen for their unique orbital arrangement. Shielded 4f shell orbitals are excited during the photoluminescence process and result in sharp-line emission peaks. Since this shell is blocked by outer electron orbitals of 6s and 5d, little or no influence is attributed from the host. This is the cause of the spectral transitions and those transitions are responsible for the emission of light which covers the range of ultraviolet to far infrared. Co-doping rare-earth elements together has also be analyzed in similar studies. In this work, co-doped erbium and ytterbium on the same aluminum nitride film has been used. In the literature, two possibilities have been explored as to why co-doped materials increase in magnitude at some peaks. The two methods by which

this could happen is either by direct excitation from one rare-earth element or some mechanism of energy transfer. Direct excitation is generally eliminated given the intensity of the laser and de-excitation from the suspected rare-earth element itself. Since the laser intensity is many orders higher in intensity than emission from the rare-earth element, it is not logical to imply that the rare-earth element has the same power as the laser and can excited its co-doped counterpart. Energy transfer seemed a more likely candidate for co-doped materials with a new peak magnitude. The two most common theories for the transfer of energy has been reported by Forester and Dexter. Both of these theories depend on the cross section of the rare-earth elements being very close to each other, increasing the probability of energy transfer [17 – 19]. In both theories, overlapping cross sections of emission σ_{em} and absorption σ_{abs} are key factors in expressing a critical radius R_{sx} where s stands for sensitizer and x stands for either s in case of energy migration between sensitizers or for acceptor in case of energy transfer from sensitizers. Eqn. 1.1 describes this relationship with c as the speed of light, τ_s as the florescence decay time, and n as the refractive index [17 – 19].

$$R_{sx}^6 = \left(\frac{3c\tau_s}{8\pi^4 n^2}\right) \int \sigma^s_{em}(\lambda)\sigma^x_{abs}(\lambda)d\lambda$$

(1.1)

The classic theory of Forster-Dexter assumes that sensitizers and acceptors are randomly and uniformily distributed and that sensitizers play no role in the interaction. Florescence decay follows from an exponential form which results in no influence of sensitizer concentration on decay time. When the overlap integral from Eqn. 1.1 gives a non-zero result, the probability of energy transfer is no longer zero between two ions. The energy transfer rate, however, varies as the fraction of radii, $(R_{sx}/R)^6$. This implies a drastic

change in energy transfer when the distance R approaches the critical radius, $R_{sx.}$ The transfer probability can be mathematically described by Eqn. 1.2 where R is the separation distance between the donor and acceptor, R_o is the critical separation, and s indicates dipole-dipole, dipole-quadrupole, and quadrupole-quadrupole interactions [17 – 19].

$$W = \sum_{s=6,8,10}^{'} [\frac{1}{\tau_s}(\frac{R}{R_o})^s]$$

(1.2)

If a donor is surrounded by randomly distributed acceptors, a new relation is used to invovle the acceptor concentration (n_a) and the dipole-dipole interaction parameter between the energy donor and acceptors (C). This relationship is shown below in Eqn. 1.3.

$$\Phi(t) = \Phi(0) e^{[\frac{-t}{\tau_s} - n_a(\frac{16\pi^3 Ct}{9})^{\frac{1}{2}}]}$$

(1.3)

If we consider the time it takes for energy to migrate among sensitizers until it finds acceptor ions, another model can be included. This model was created and named after Burshtein [19] which focuses on energy migration between sensitizers. Concentrations of sensitizers and acceptors are the two major factors that play a role in this model with florescence decaying at an exponential rate. Eqn. 1.4 shows this relationship. Furthermore, in this paper co-doped erbium and ytterbium will be studied and analyzed based off these two possible methods.

$$W = n_s n_a [\frac{\pi R_{sa}^3 R_{ss}^3 (\frac{2\pi}{3})^{\frac{5}{2}}}{\tau_s}]$$

(1.4)

Biomedical applications can be used based off the research shown here by using rare-earth elements as isotopes to illuminate cancer underneath the skin. Nanoparticles are also being researched involving rare-earth elements for this reason. Harmless effects used in conjunction with the body are always a popular research area in the medical physics field. Applications of a magnetic field (which does not harm the body) has gained certain interest and research is underway involving its effects on optical and luminescence properties. Research done in this paper furthers the study of the effects from a magnetic field on certain rare-earth elements optical properties. Past research has shown a split in the degeneracy levels causing spectrum peaks to be split. The research shown at the end of this paper will confirm peak splitting and also investigate a new phenomenon of the magnetic field's effect on the peak magnitude. Device fabrication is also a possibility from population inversion by co-doping materials together.

Chapter 2

2.1   Nitride Semiconductors

Semiconductors are most commonly known for their integrated role in electronic devices. However, nitride semiconductors are unique in that they are being studied more for their contributions to modern science in the field of optics as opposed to other semiconductors. Both, optical and electrical properties are being developed based on research working with different types of nitride semiconductors [1 – 4, 20]. Due to their properties (such as high thermal conductivity, energy bandgap, and melting point), they make excellent host films for luminescent materials. Most nitride semiconductors have similar properties to each other; however, three major factors vary within this distinctive family of devices. AlN, GaN, InN, and BN are more commonly used nitride semiconductors.

At high temperatures, these devices carry unique properties that are different than at room temperature. Unfortunately, this makes some of the nitride semiconductors unsuitable for electronically dominated systems [18, 22 - 25]. Another exciting research area that separates nitride semiconductors from one another is their energy band gap. Each nitride semiconductor has its own bandgap, capable of sustaining many different elements to study optical and luminescence properties of those elements [6 - 12, 25]. In recent years, the nitride semiconductor GaN has gained special attention for its large band

gap compared with the more common, silicon semiconductors [18, 22 - 25]. The crystal structure of each nitride semiconductor is also a well documented property. The three most common crystal structures are given as wurtzite, zincblende, and rock-salt. Crystal structure depends on the temperature and pressure at which the nitrides were synthesized. Figure 2.1, 2.2, and 2.3 demonstrate each crystal structure. Wurtzite is primarily a hexagonal shape although Figure 1.1 shows only a unit cell. Zincblende and rock-salt crystal structures both have a unit cell based off the face centered cubic lattice. However, zincblende has its crystals offset so that they make a diamond shape. Rock-salt crystals have a strictly cubic (octahedron) pattern.
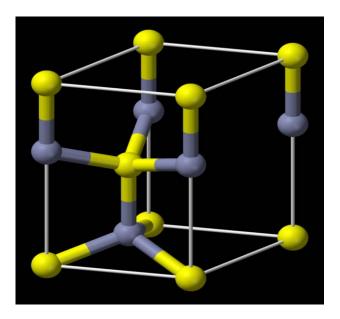

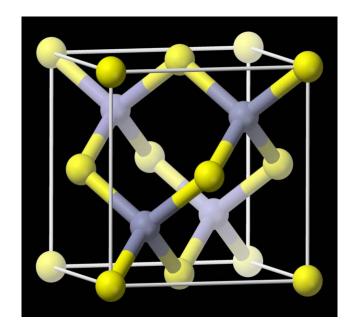**Figure 2.1.** *Wurtzite crystal structure [25].*

Figure 2.2. *Zincblende crystal structure [25].*
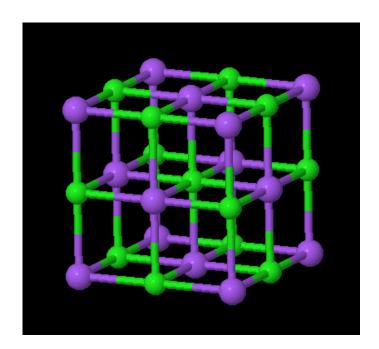
Figure 2.3. *Rock-salt crystal structure [25].*

2.2   Common III-Nitride Semiconductors

The four most common nitride semiconductors being studied today are aluminum nitride (AlN), boron nitride (BN), gallium nitride (GaN), and indium nitride (InN). Each has its own interesting properties which stem from the way it was synthesized, temperature tolerances, crystal structure, and bandgap values.

AlN has been used in many different optoelectronic devices since its fabrication in 1877 [25]. Although it was first created many years ago, its value is becoming more obvious for its use in the optical field. Considering its hardness, high thermal conductivity, high temperature tolerance, and bandgap, it has recently been considered as a valuable component in electronic devices and photoluminescence studies. AlN generally has a crystal structure of wurtzite but also exists in an amorphous state [18, 22 - 25].

BN has one defining property in that its crystal structures vary widely and include one uncommon crystal type. Two of the common crystal types can be made (wurtzite and zincblende) but also hexagonal BN (similar to graphite) can be created by different methods. The band gap is relatively high in comparison to the other nitride semiconductors; however, it varies widely depending on the crystal structure [18, 22 - 25].

GaN is the most common of the nitride semiconductors and has been the most studied. Current uses include LED's, DVD player/recorders, mobile phones, and UV emitters [22, 23]. One of the most useful properties of GaN is that its band gap is very high

compared to silicon and it is easy to create. Although this can be formed in two different ways (wurtzite and zincblende), its bandgap is still around the same value [18, 22 – 25].

InN is the most difficult to grow, which makes it impractical for use as a semiconductor. Large numbers of impurities and the inability to grow at high temperatures indicate that InN is not a good choice for research. The crystal structure that is formed is hexagonal in nature, representing wurtzite [18, 22 - 25]. Furthermore, alternative and easier ways to create semiconductors are present with a similar bandgap value that makes InN impractical.

As mentioned before, a higher bandgap is crucial in determining which nitride semiconductor is suitable for a particular research [5 - 12]. Bandgaps are based off the element that is synthesized to grow the nitride semiconductor. Variances have occurred in some room temperature energies. However, comparison of each bandgap with each nitride semiconductor is shown in Table 2.1. Some nitride semiconductors have more than one crystal structure, which in turn affects the bandgap energy. Each crystal structure is listed when appropriate.

Table 2.1. *Specific bandgap energy levels for each nitride semiconductor [25].*

Material	Crystal Structure		
	Wurtzite	Zincblende	Hexagonal
AlN Energy gap (eV)	6.2	NA	NA
BN Energy gap (eV)	4.5 - 5.5	6.1 - 6.4	4.0 - 5.8
GaN Energy gap (eV)	3.39	3.2	NA
InN Energy gap (eV)	1.89 - 2.05	NA	NA

2.3   Aluminum Nitride

Given the bandgap energies from Table 2.1, AlN is one of the better choices to study. AlN was also chosen due to the lack of studies being done involving this particular nitride semiconductor with rare-earth elements involving both infrared and green laser excitation. Research done here focuses on photoluminescence using AlN as a reliable host. Useful AlN properties are shown below in Table 2.2. Although not all properties are used in this paper, they are listed here for completeness.

Table 2.2. *Basic properties of AlN including electrical, thermal and mechanical, and optical [25].*

Basic Parameters:

Crystal Structure		Wurtzite
Number of atoms in 1 cm^3		9.58×10^{22}
Debye Temperature(K)		1150
Density(g cm^{-3})		3.23
Dielectric Constant:		
Static		8.5
High Frequency		4.6
Effective electron mass (in units of M_o)		0.4
Effective hole mass (in units of M_o):		
Heavy		
for k_z direction	M_{hz}	3.53
for k_x direction	M_{hx}	10.52
Light		
for k_z direction	M_{lz}	3.53
for k_x direction	M_{lx}	0.24
Split-off Band		
for k_z direction	M_{soz}	0.25

for k_x direction	M_{sox}	3.81
Electron Affinity (eV)		0.6
Lattice Constant (Å)		a = 3.112
		c = 4.982
Optical Phonon Energy (meV)		99
Energy Gap (eV)		6.2
Energy of Spin-Orbital Splitting E_{so} (eV)		0.019
Effective conduction band density of states (cm^{-3})		6.3×10^{18}
Effective valence band density of states (cm^{-3})		4.8×10^{20}

Electrical Properties:

Breakdown Field (V cm^{-1})	$(1.2 \div 1.8) \times 10^6$
Mobility (cm^2 V^{-1} s^{-1}):	
electrons	300
holes	14
Diffusion Coefficient (cm^2 s^{-1})	
electrons	7
holes	0.3
Electron thermal velocity (m s^{-1})	1.85×10^5
Hole thermal velocity (m s^{-1})	0.41×10^5

Optical Properties:

Infrared refractive index	2.15
Radiative recombination coefficient (cm^3 s^{-1})	0.4×10^{-10}

Thermal and Mechanical Properties:

Bulk Modulus (dyn cm^{-2})	21×10^{11}
Melting Point ($^{\circ}$C)	2750 (between 100 and 500 atm of nitrogen)
Specific Heat (J g^{-1} $^{\circ}$C)	0.6
Thermal Conductivity (W cm^{-1} $^{\circ}C^{-1}$)	2.85
Thermal Diffusivity (cm^2 s^{-1})	1.47
Thermal Expansion, Linear ($^{\circ}C^{-1}$)	$\alpha a = 4.2 \times 10^{-6}$
	$\alpha c = 5.3 \times 10^{-6}$

Chapter 3

3.1   Rare-earth Elements

Rare-earth elements have unique characteristics unlike most other elements on the periodic table. These consist of thirty elements all together separated into two different groups, lanthanides (fifteen total) and actinides (fifteen total). The lanthanide are elements famous for their 4f shell level that resides deep inside the atom itself. Each lanthanide contains a 4f orbital shielded by 4d and 5p orbital electrons. The transitions of these elements by excitation and de-excitation cause emissions which are detected in the infrared, visible, or ultraviolet region [23 - 25]. All lanthanides have an electron configuration resembling Xenon with additional electrons in the 6s, 5d, and 4f orbitals. Table 3.1 shows the series of fifteen different rare-earth elements known as lanthanides and their electron configuration. Most lanthanide elements have a configuration filling the 6s level and 4f levels with a few exceptions. All lanthanides have an ionization of 3+ which makes them excellent for doping with an aluminum nitride semiconductor. Only three different lanthanides are studied in this paper including erbium, terbium, and ytterbium.

Table 3.1. *Lanthanide elements listed with appropriate electron configurations [26].*

Atomic Number	Lanthanide	4f Electrons	Configuration
57	Lanthanum	0	[Xe] $5d^1$ $6s^2$
58	Cerium	2	[Xe] $4f^2$ $6s^2$
59	Praseodymium	3	[Xe] $4f^3$ $6s^2$
60	Neodymium	4	[Xe] $4f^4$ $6s^2$
61	Promethium	5	[Xe] $4f^5$ $6s^2$
62	Samarium	6	[Xe] $4f^6$ $6s^2$
63	Europium	7	[Xe] $4f^7$ $6s^2$
64	Gadolinium	7	[Xe] $4f^7$ $5d^1$ $6s^2$
65	Terbium	9	[Xe] $4f^9$ $6s^2$
66	Dysprosium	10	[Xe] $4f^{10}$ $6s^2$
67	Holmium	11	[Xe] $4f^{11}$ $6s^2$
68	Erbium	12	[Xe] $4f^{12}$ $6s^2$
69	Thulium	13	[Xe] $4f^{13}$ $6s^2$
70	Ytterbium	14	[Xe] $4f^{14}$ $6s^2$
71	Lutetium	14	[Xe] $6s^2$ $4f^{14}$ $5d^1$

3.2   Erbium, Terbium, and Ytterbium

The three rare-earth elements studied include Erbium, Terbium, and Ytterbium. Little work has been done in analyzing these specific elements with an AlN semiconductor. The co-doping of Erbium and Ytterbium is also analyzed in this paper to study the effects both of them have together. Electron orbital properties were found from the previous listing in Table 3.1. More basic properties including melting/boiling points, density, and ionization energies are reported in Table 3.2 for all three elements [27, 28].

Most properties are similar, however; Ytterbium has a melting point at such a low value that the temperature range for liquid is relatively small.

Table 3.2. *The three rare-earth elements listed with common properties [28].*

Property	Rare-earth Element		
	Terbium	Erbium	Ytterbium
Atomic Mass (g/mol)	158.93	167.26	173.04
Electronegativity	1.2	1.24	1.1
Melting Point (◦C)	1356	1529	824
Boiling Point (◦C)	3230	2868	1196
Density (g/cm3)	8.23	9.066	9.321
Molar Heat Capacity (J/mol K)	73.2	28.12	26.74
Standard Molar Entropy (J/mol K)	28.91	73.2	59.9
Ionization Energy (kJ/mol)			
First	565.8	589.3	603.5
Second	1110	1150	1174.8
Third	2114	2194	2417

Each element has different transitions that the 4f shell is capable of. Such transitions are responsible for the emission that this research is focused on. A graphical representation of the energy levels was made and is displayed in Figure 3.1 with all three elements listed [15, 16].
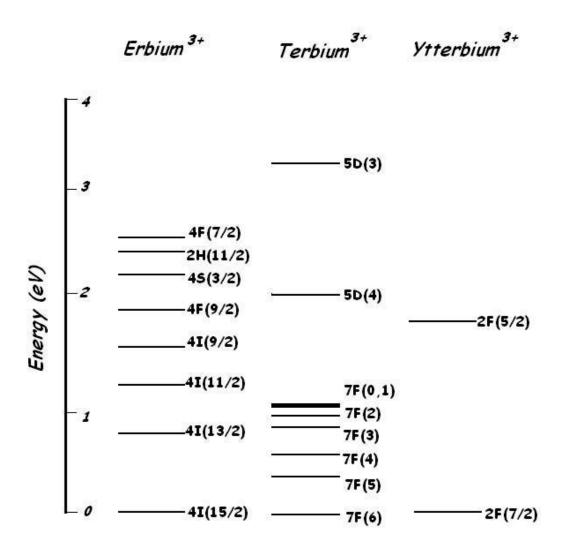
Figure 3.1. *Energy level diagrams for Er^{+3}, Tb^{+3}, and Yb^{+3}.*

Chapter 4

4.1   Methodology and Experimental Setup

Materials studied in this work are in the form of thin films grown by an rf sputtering technique. The sputtering technique has been known and used for many years. In general, sputtering removes surface atoms of a target by using ions of a particular gas and incident particles. It is necessary to describe this process to better understand the experimental setup. Previous authors [1 - 10] have detailed the method outlined below.

The thin films used here including AlN: Er, AlN: Tb, AlN: Yb, and AlN: ErYb were prepared on silicon substrates using the method of rf magnetron sputtering with a target of 99.999% purity with a 5.1 cm diameter piece of aluminum. The rare-earth elements were incorporated into Al by drilling a hole in the aluminum target, approximately 0.5cm in diameter and placing a small amount of the rare-earth element inside. In the case of AlN: ErYb, two separate amounts of both elements were placed inside Al by drilling two holes. Both were then co-sputtered together in a chamber. The rf power was kept between 100 – 200 watts with the chamber pressure set below 0.00003 Torr. To start the process, plasma must be created from the gas inside a small chamber, using nitrogen in this case. A voltage difference is applied from the plasma gas and the target resulting in the acceleration of ions from the plasma onto the target. From this,

atoms on the surface of the target are ejected by the momentum of the ions (only if the energy of the ions is higher than the sputtering threshold of approximately 20 eV). More ions are created to maintain the plasma process by ion surface interactions at the negative electrode. All of this was done at a temperature of 77 K using a completely nitrogen atmosphere. Liquid nitrogen was used to ensure the temperature remained constant at 77 K. A magnetic field is used perpendicular to the substrate to ensure a constant bombardment of the target with the ionized gas atoms. This magnetic field also increases the number of ionized gas particles which in turn improves the quality of the deposited film. Thicknesses of the films were analyzed by a quartz crystal thickness monitor. The film thickness used here are between 200nm – 400nm. Surface characterization was determined using XRD (X-Ray Diffraction). Diffraction peaks were observed which indicates these films are amorphous [1 - 10].

For photoluminescence, a spectrometer (Model Number SP2300i) made of Princeton Instrumentation; equipped with a photomultiplier tube was used in conjunction with a program called *Winspec*. Each film was attached to a post at the same height as the opening on the spectrometer while a laser set atop an adjustable bench. The two lasers used for excitation were a 532nm Nd:YAG green solid state laser and 783nm infrared solid state crystal laser. For each experiment, the laser, film, and slit opening to the spectrometer were set at identical angles. Approximately a 40° angle was used relative from the laser beam to the film which produced a 10° angle to the detector relative to the normal. Angle parameters were adjusted to be the same as for the both 532 nm green laser and 783 nm infrared laser (40° and 10°). An overview of this setup is shown in

Figure 4.1. A magnetic field was also applied to study and observe energy level splitting in some cases. This is also shown in Figure 4.1. The opening on the spectrometer used a micrometer to adjust the opening of the light coming into the detector. After the data were collected, Microsoft Excel 2003 was used to convert the files into an appropriate format for easier display.

After the film and laser have been placed accordingly, the laser was then turned on and reflected off the film into the spectrometer. Both lasers were designed so that overheating did not play a crucial role in the results. Hence, the lasers were left on for the duration of the experiment for each setting and turned off at the end of each session. The program *Winspec* took data in separate scans at different regions and then glued them together. Each scan appeared within a matter of seconds. The typical unit of intensity is the candle (cd) however here we use units that make no distinction to a set value. Each scan recorded is then stitched together to math other inregion the intensity in a.u. (arbitrary units) where the intensity is only dependent on how much light is shining through. Each spectrum is then redefined to eliminate unnecessary data for each figure. Data beyond the ranges shown in the results section were simply background and were cut to show only the important regions. Spectra only focus on parts which show peak values.
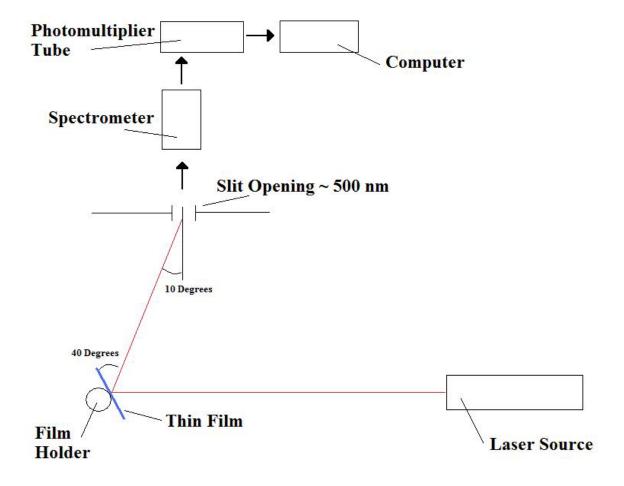
Figure 4.1. *Overview drawing of experimental setup.*

4.2   Resolution and Error Analysis

Error analysis was conducted using methods outlined by Taylor in the literature [28]. Using Eqn 4.1, error for each spectrum was calculated. Error bars are displayed in certain figures when applicable.

$$\sigma = N^{1/2} \tag{4.1}$$

Sigma represents the error at the point of N where N stands for the total intensity at that specific point.

Also, the slit of the spectrometer is a key factor in how the data is taken. Resolution is determined by the opening of the slit on the detector. The slit was chosen to display the best results with the finest spectrum peaks. When the slit was increased, the resolution decreased however the intensity of light was amplified. This amplification in intensity is due to the higher number of photos entering the detector. The wider slit width decreased the resolution since the detector has difficulty distinguishing between different energy levels. If the slit is set at a low value, the detector will be able to focus on a more accurate resolution; however, the peak intensity will suffer a decrease in magnitude. This is due to the fact that less light is coming into the detector and it can more accurately distinguish specific energies from each other. Also, background was subtracted for each spectrum.

Chapter 5

5.1   Results and Analyses

This chapter discusses the results of doped AlN with the three different rare-earth elements listed previously. In each section of the chapter, a spectrum of each rare-earth element using photoluminescence is shown to indicate peak values given at certain wavelengths. Emission peaks are identified and refer to the known energy levels of each rare-earth element [15 – 17]. A table of energy values corresponding to each detected wavelength is also given. Furthermore, a magnetic field was applied to each film at different angles to experiment with intensity output and peak shifting. Those spectra along with peak values are also reported in both energy and wavelength. Spectral emissions along with known energy levels for each rare-earth element are compared.

5.2   Erbium

Thin films of Erbium doped AlN are characterized for their luminescence using a green laser (532 nm) and an infrared laser (783 nm). The luminescence spectrum from Erbium was studied within the range of 540 nm to 1560 nm, with peaks observed at 554 nm and 561 nm using the green laser. The magnitude of the first peak is approximately

six times the peak of the second one. Figure 5.1 shows the photoluminescence spectrum of AlN: Er at room temperature with the green laser with low peaks. Figure 5.2 displays the spectrum using the 783 nm infrared laser. The only peak detected here was 1553 nm. Since the infrared laser is of lower order intensity, more error in the spectrum is shown by a non-smooth curve and the peak magnitude is lower than that from the green laser. Energy for each peak was found using the relationship between energy, wavelength, and the two constants, the speed of light and Planck's constant, shown below:
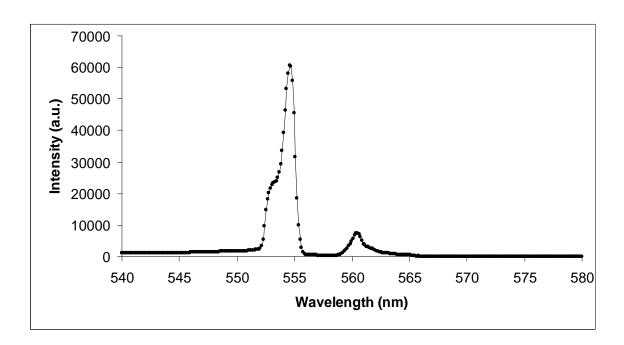
$$E\lambda = hC \tag{5.1}$$

Figure 5.1. *Photoluminescence spectrum of AlN: Er film excited by a 532 nm laser.*

Using Eqn 5.1, each peak on the spectrum was converted into a corresponding energy. The factor *hc* (the conversion between energy and wavelength) was taken to be

1240 eV nm. Energy transitions were then identified as the source of each peak using the known energy level transitions. Since the intensity of the infrared laser is much lower than the green laser, the opening on the detector was increased to 200 µm. Figure 5.2 shows the spectrum taken at room temperature with the infrared laser.
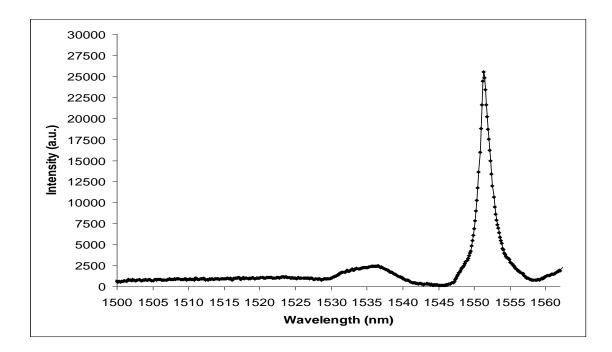

Figure 5.2. *Photoluminescence spectrum of AlN: Er film excited by a 783 nm laser.*

Spectrum peaks included are summarized in Table 5.1 for both the green and infrared laser for Erbium. Relative intensity values correspond to the relative height of each peak to one another. This also indicates how frequent the energy transitions occurred in comparison with each energy level. Using the energies calculated from each wavelength, energy transitions were compared and confirmed for each rare-earth element.

Table 5.1. *Tabulated values of emissions for Er ions for both green and infrared lasers.*

Erbium			
532 nm Laser	Wavelength (nm)	Energy (eV)	Transition
	554	2.250	$^2H_{11/2} \rightarrow \ ^2I_{15/2}$
	561	2.210	$^4S_{3/2} \rightarrow \ ^4I_{15/2}$
783 nm Laser	Wavelength (nm)	Energy (eV)	Transition
	1552	0.793	$^4I_{13/2} \rightarrow \ ^4I_{15/2}$

5.3 Ytterbium

Ytterbium contains unique peak values in its spectrum similar to that of Erbium. The spectrum was again taken to be within 540 nm to 1560 nm for the green laser and 800 nm to 1560 nm for the infrared laser. Peak values here were analyzed in the same way and were detected at 966nm for the green laser. This peak is broader and spans the region from 963nm to 969nm. Given the conversion factor between peaks and energy, a table of values was deduced corresponding to energy emission. No detectable peaks were given in the infrared. The same setup was used as for Erbium including the angles between the laser, film, and detector. The opening slit on the detector was adjusted for the best peak results at 100 µm and 250 µm for the green and infrared laser respectively. Also, the scan includes a large spectrum, but only the parts that are showing clear peak are shown. Figure 5.3 shows the green spectrum with the transition peaks indicated. The transition for the peak at 966 nm is determined to be $^2F_{5/2}$ to $^2F_{7/2}$ with an energy

corresponding to 1.284 eV. Error bars are applied here to show that different energies are present for this one transition.
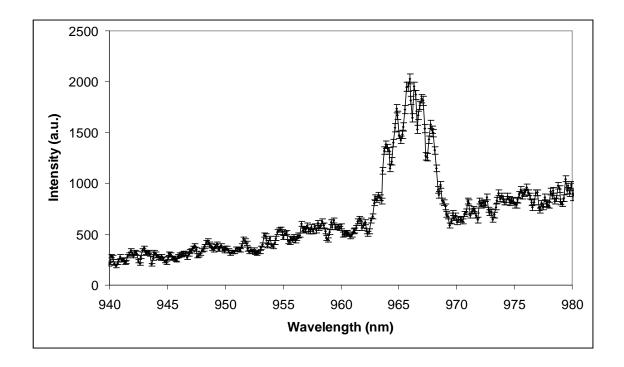

Figure 5.3. *Photoluminescence spectrum of AlN: Yb film excited by a 532 nm laser.*

5.4 Terbium

Terbium was also evaluated in the same way as described above. The spectrum given in Figure 5.5 gives the results of this film using a green laser only. Figure 5.6 shows the results from using the infrared laser. Spectral ranges were kept the same as before and peak values occurred mainly at 549 nm and 562 nm for the green laser. There are two detectable peaks using the infrared at 1533 nm and a broad peak centered on 1508 nm. Terbium produced strong emission using the green laser, so the slit opening

was only adjusted to 25 µm. Since the infrared laser has such low intensity, a slit opening

of 150 µm was used. Table 5.3 shows the relative peaks along with corresponding energy

transitions for Terbium.

Table 5.2. *Tabulated values of emissions from Tb ions for both green and infrared lasers.*

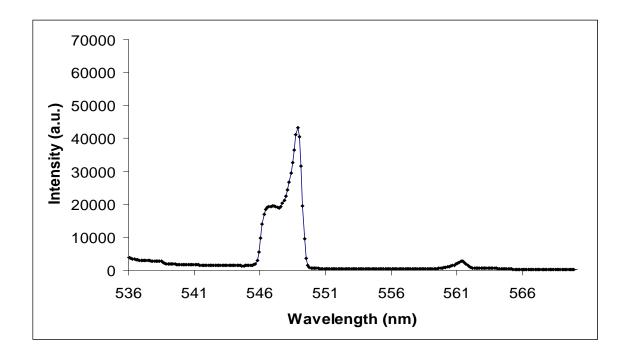| Terbium			
532 nm Laser	Wavelength (nm)	Energy (eV)	Transition
	549	2.259	$^5D_4 \rightarrow {}^7F_5$
	562	2.206	$^5D_4 \rightarrow {}^7F_4$
783 nm Laser	Wavelength (nm)	Energy (eV)	Transition
	1508	0.822	$^5D_2 \rightarrow {}^5D_4$
	1533	0.809	$^5L_9 \rightarrow {}^5D_4$

Figure 5.4. *Photoluminescence spectrum of AlN: Tb film excited by a 532 nm laser.*
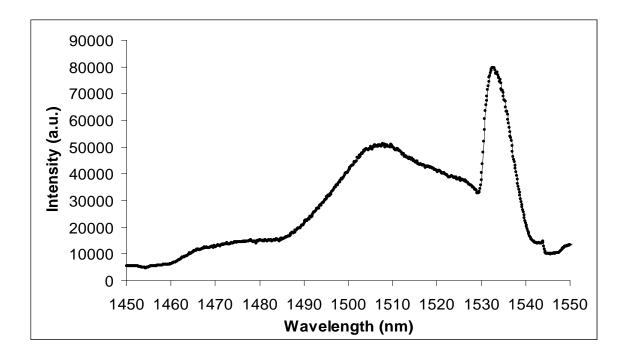
Figure 5.5. *Photoluminescence spectrum of AlN: Tb film excited by a 783 nm laser.*

5.5 Interaction of Erbium and Ytterbium

Upon doing research with erbium and ytterbium, work has been done in the past that indicates the mixture of two rare-earth elements may change the properties of the semiconductor. A new film, erbium and ytterbium were both doped into the aluminum nitride semiconductor. This new film was analyzed in the same way as before using the same angle setup. The slit width on the detector was set at 50 µm for the green laser and 75µm for the infrared. Figure 5.7 gives the results of the green laser excitation for this film including the prominent peak at 556 nm and the smaller peak at 561 nm. This is similar to the erbium spectrum which showed two peaks in roughly the same areas. Figure 5.8 shows another peak using the green laser that is not nearby the previous two

peaks. This peak at 968 nm appears narrower than the broader peak of just ytterbium alone. Figure 5.9 shows the infrared laser results with a single peak at 1567 nm. This peak has an increased magnitude, but shifted from just Erbium alone. Table 5.4 shows energy transitions and levels along with corresponding peaks.

Table 5.4. *Tabulated values of emissions from Er and Yb ions for both green and infrared lasers.*

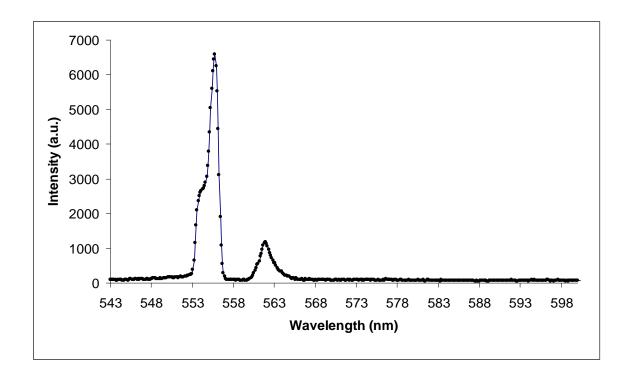| Erbium and Ytterbium			
532 nm Laser	Wavelength (nm)	Energy (eV)	Transition
	556	2.230	$^2H_{11/2} \rightarrow {}^2I_{15/2}$
	561	2.210	$^4S_{3/2} \rightarrow {}^4I_{15/2}$
	968	1.281	$^2F_{5/2} \rightarrow {}^2F_{7/2}$

Figure 5.6. *Photoluminescence spectrum of AlN: ErYb film excited by a 532 nm laser.*
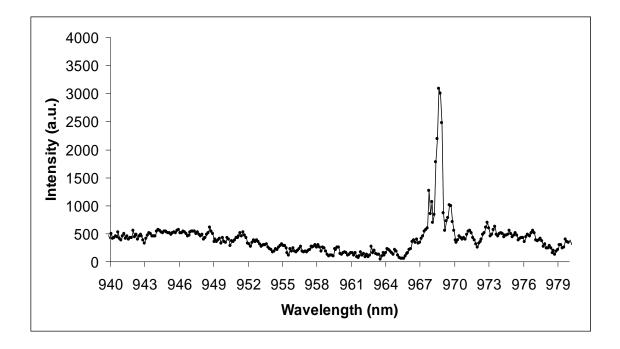

Figure 5.7. *Photoluminescence spectrum of AlN: ErYb film excited by a 532 nm laser.*

Another interesting property that was studied with the erbium and ytterbium aluminum nitride semiconductor is the effect of a magnetic field. This magnetic field was applied to all four different films however, only the AlN: Er and Yb has a noticeable effect. A magnetic field of 0.1 T was applied in the perpendicular and parallel direction to the film although both gave the same results. Figure 5.10 shows the results of the magnetic field on the peaks at 561.0 nm and 554.6 nm). The peak at 968 nm did not show a noticeable effect using the magnetic field applied nor did the infrared peak. For comparison, the same angles and slit widths were used (no parameters different).
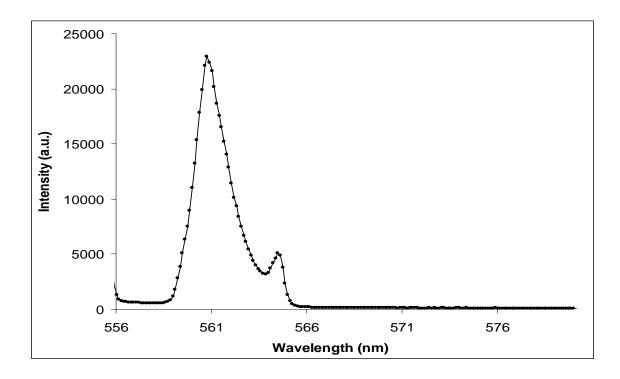
Figure 5.8. *Photoluminescence spectrum of AlN: Er film with a magnetic field.*

Chapter 6

6.1   Discussion

Results for each film with green and infrared laser excitation are shown in Figures 5.1 – 5.10. From these, spectral peaks have been assigned based off the conversion from wavelength to energy using the relationship given in section 5.2. Two major results will be discussed below involving the comparison between AlN: Yb, AlN: Er, and AlN: ErYb and the effect of the magnetic field.

From the data, erbium has several known transitions after being excited by the green laser. Energy transfer was also observed from erbium to ytterbium when both are co-doped together in AlN. To discuss the energy transfer phenomenon, comparisons were made using information from the AlN: Yb weak emission at 966 nm. There are two ways in which erbium can enhance the IR emission of ytterbium: direct excitation by erbium green emission and energy (electron) transfer from erbium into ytterbium. The green emission from erbium is energetically strong enough to cause a direct excitation in the ytterbium. Therefore the luminescence enhancement in ytterbium could be either due to one of the two phenomena or due to both phenomena. The first method, direct excitation by green emission from erbium, was eliminated based off the following argument. The intense green laser produces a very weak IR emission at 966 nm in ytterbium. The green

emission from erbium is negligibly weak in intensity and power compared to the excitation laser while our experimental results show that the intensity of the luminescence almost doubles when erbium is codoped with ytterbium. In that case, approximately half of the intensity would be produced by the extremely high power green laser and the remaining half by an almost same wavelength but negligibly weaker green emission of erbium. Technically, this is not possible. The excitation spectra are usually broad, so if the green emission from erbium at 554nm is in the excitation range of the ytterbium, then 532nm green laser also falls in the excitation region of the ytterbium. Therefore, it eliminates the possibility that a 532nm laser does falls in the excitation wavelength range of the ytterbium. Thus, a direct excitation of ytterbium by the erbium green emissions has not occurred. The only other option left behind is the energy transfer from erbium to ytterbium. Therefore, this analysis shows that erbium and ytterbium interact with each other when doped together in amorphous AlN film and give an energy transfer process in erbium and ytterbium ions.

An interesting application of the energy transfer could be the population inversion and construction of laser cavity in ytterbium. Since the electron transfer phenomenon from erbium to ytterbium increases the population of electrons in the first excited state of ytterbium, it is possible that a stage may reach the number of electrons in the first excited state of ytterbium and could be more than the number of electrons in its ground state. At that time, a population inversion would occur and we would be able to make a 4-level laser cavity in the erbium and ytterbium ions system. Combining both rare-earth elements

together on the same semiconductor and comparing data indicates that erbium and ytterbium have interacted with the de-excitation of each other.

The normal transition is from 4S(3/2) to 4I(13/2). However, in the presence of ytterbium, electrons also transfer energy to the nearby ytterbium peak, thus increasing its output. Figure 6.1 indicates the different transitions possible and the jump from erbium de-excitation to ytterbium de-excitation. The jump of energy is shown by the curved arrow in Figure 6.1. Energy is transferred by electrons coming from erbium and de-exciting to a ytterbium nearby. The electron then de-excites from ytterbium, causing more de-excitation from ytterbium and less from erbium. The method by which this is possible is defined as a combination between FRET and DET (Foster Resonance Energy Transfer and Dexter Energy Transfer) [17 – 19]. Due to the close proximity, the rare-earth atoms follow the FRET and DET theories of overlapping cross sections in between the atoms, causing them to exchange electrons.
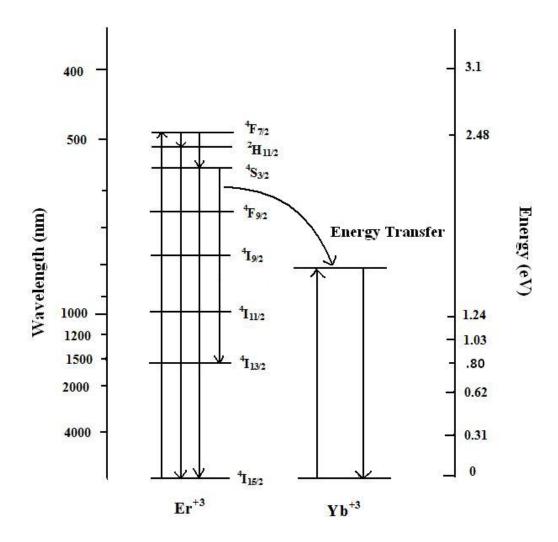
Figure 6.1. *Graphical representation of the energy transfer from Er^{+3} to Yb^{+3}.*

This portion of energy that is transferred to ytterbium increases the output of the peak detected at that range, 966nm. Qualitative comparison of this is seen in Figure 6.2 with both AlN: Yb film and AlN: Er and Yb films shown. The background detection was minimized to approximately the same level (in arbitrary units). Noticeable features are the differences in peak intensity and peak width. The introduction of erbium onto the film has increased the intensity and sharpened the peak. Increased intensity was attributed to

the previous discussion however the sharpened peak indicates the lifetime for the electron

has centered on a short value. Since co-doped erbium and ytterbium force ytterbium to

have more emission, the length of time that an electron de-excite shortens. Another clear

result from these data is the center peak shift. AlN: Yb is centered on 966 nm while the

AlN: ErYb centers at 968 nm. A peak shift indicates that Erbium has disturbed the energy

levels of Ytterbium, and the energy is slightly perturbed from the original spectrum. Data

from the 551 nm/561 nm region were also analyzed in the same way as before. The

energy taken from erbium decreased the peak at 554 nm, however, since the intensity of

that peak is so great, a small decrease is nearly undetectable compared to the large

increase at 968 nm.

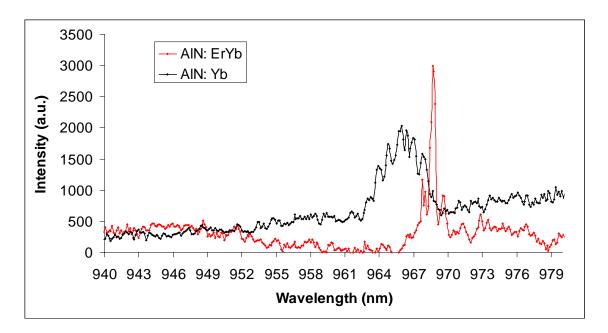

Figure 6.2. *Luminescence enhancement in AlN:Yb by co-doped erbium.*
.

The effect of the magnetic field was investigated for the AlN: ErYb film and is

shown in Figure 5.10. To ensure the same parameters, the slit width and angle setup were

kept the same. Background intensity was kept level for the same arbitrary units (similar to before). Both spectra were put on the same graph and set in Figure 6.3 below. As shown, the peak at 561nm has minor splitting with a smaller peak at 564nm. This is consistent with the research that has been done before with a magnetic field. The intensity of the main peak at 561nm has also increased due to the magnetic field's effect. This increase in intensity is a new phenomenon that needs further study. Since magnetic fields are not harmful to the human body, increased emission could also prove to be very useful in detecting cancerous cells underneath the skin.
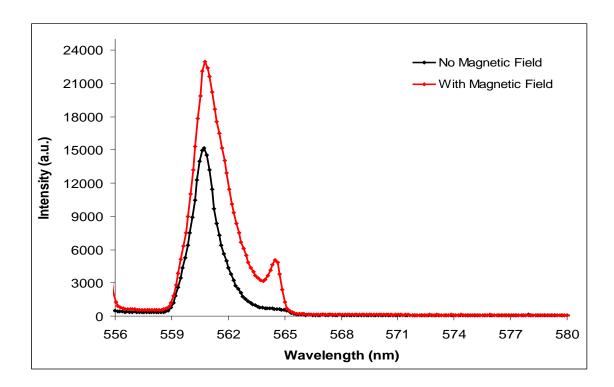

Figure 6.3. *Photoluminescence of AlN: ErYb with both a magnetic field and without a magnetic field.*

6.2   Conclusion

Four films were studied (AlN: Er, AlN: Yb, AlN: Tb, AlN: ErYb) by the method of photoluminescence from laser excitation with both green and infrared lasers. Thin films created by rf magnetron sputtering have been used to dope rare-earth elements (all of which are lanthanides) onto a nitride semiconductor with the film for research. Using a 532 nm green laser and 150 nm infrared laser, excitation and de-excitation were measured using a spectrometer for each film. Each film has detectable peaks displayed in Chapter 5.

Erbium and ytterbium were evaluated separately and then analyzed together. Comparisons were made from each element alone in contrast to both elements' interaction on each other. Ytterbium was concluded to have a broad peak centered at 966 nm, while the interaction of both erbium and ytterbium produced a sharp peak centered at 968 nm with a higher intensity. This increase in intensity suggests energy transfer from erbium to ytterbium. As noted in section 6.1, the energy transfer increased the number of de-excitations occurring from ytterbium and thus increases the output intensity at that peak. The peak shift and change from broad to sharp still needs further study.

The AlN: ErYb film was also studied under the influence of an external magnetic field. With a magnetic field, the peak centered at 561 nm split into a major peak at 561nm and a minor peak at 564 nm. An increase in intensity was also observed which is still being studied. Biomedical fields may consider this research valuable in detecting cancer under the skin or deep within the body. Infrared and other high energy lasers, which

penetrate the body easily, may play an important role if used with strongly emitting lanthanides.

In the future, additional research should be done in the field of optical and luminescent properties of rare-earth elements. Nitride semiconductors play excellent hosts given their wide bandgap in comparison to other materials. Doping different combinations of lanthanides together could also be worthwhile to study, being that we are unaware of the energy transfers between any two elements. Another rising use for the study of these elements may be in electronics (since we are working with semiconductors). Unique properties make these new materials valuable for the creation of higher-strength magnets, batteries, or even computers. A more promising field is using the photoluminescence research to treat cancer using the rare-earth element as an isotope. With more research, the photoluminescence could prove useful in detection and treating patients with cancer by using lasing techniques to see emission under the skin [29].

References

1. M. Maqbool, I. Ahmad, H. H. Richardson and M. E. Kordesch. Direct ultraviolet excitation of an amorphous AlN:Praesiodimium phosphor by co-doped Gd(+3) Cathodoluminescence, Applied Physics Letters 91, 193511 (2007).

2. M. Maqbool, Martin. E. Kordesch, and A. Kayani, Enhanced Cathodoluminescence from an amorphous AlN:Holmium phosphor by co-doped Gd(+3) for optical devices applications, Journal of the Optical Society of America-B 26, 998 (2009).

3. M. Maqbool, E. Wilson, J. Clark, I. Ahmed and A. Kayani, Luminescence from Cr(+3) doped AlN films deposited on optical fiber silicon substrates for use as waveguides and laser cavities, Applied Optics 49, 653 (2010).

4. N. Managaki, M. Fujii, T. Nakamura, Y. Usui, and S. Hayashi, Enhancement of photoluminescence from Yb and Er co-doped Al_2O_3 films by an asymmetric metal cavity, Appl. Phys. Lett. 88, 042101-042103 (2006).

5. Y. Mao, J. Y. Huang, R. Ostroumov, K. L. Wang, and J. P. Chang, Synthesis and Luminescence Properties of Erbium Doped Y2O3 Nanotubes, J. Phys. Chem. 112, 2278 (2008).

6. A. J. Steckl and R. Birkhahn, Visible emission from Er-doped GaN grown by solid source molecular beam epitaxy, Appl. Phys. Lett. 73, 1700-1702 (1998).

7. M. Maqbool , H. H. Richardson and M. E. Kordesch, Electron penetration depth in amorphous AlN exploiting the luminescence of AlN:Tm/AlN:Ho bilayers Current Applied Physics 9, 417-421 (2009).

8. V. Dimitrova, P.G. Van Patten, H. Richardson and M.E. Kordesch, Photo-, cathodo- , and electroluminescence studies of sputter deposited AlN : Er thin films, Applied Surface Science 175-176, 480-483 (2001).

9. M.L. Caldwell, A.L. Martin, C.M. Spalding, V.I. Dimitrova, P.G. Van Patten, M.E. Kordesch and H.H. Richardson, Visible emission from amorphous AlN thin-film phosphors with Cu, Mn, or Cr , J. Vac. Sci. Technol. A 19, 1894-1897 (2001).

10. F. S. Liu, Q. L. Liu, J. K. Liang, J. Luo, H. Zhang, Y. Zhang, B. Sun, and G. Rao, Journal of visible and infrared emissions from c-axis oriented AlN:Er films grown by magnetron sputtering, Applied Physics 99, 053515 (2006).

11. M.E. Little and M.E. Kordesch, Band-gap engineering in sputter-deposited $Sc_xGa_{1-x}N$ Appl. Phys. Lett. 78, 2891-2893 (2001).

12. John B. Gruber *et al*, Spectroscopic properties of Sm^{3+} ($4f^5$) in GaN. Journal of Applied Physics, Volume 91, No. 5, 2929-2935 (2002).

13. H. J. Lozykowski, Kinetics of luminescence of isoelectronic rare-earth ions in III-V Semiconductors. Physical Review B 48, 17758 (1993).

14. S. Schmitt-Rink *et al*, Excitation and optical properties of rare-earth ions in semiconductors. Physics Review Letters. 66, 2782 (1991).

15. G. H. Dieke, Spectra and Energy Levels of Rare Earth Ions in Crystals, Interscience Publishers (New York, 1968).

16. H. J. Lozykowski, W. M. Jadwisienczak, and I. G. Brown, Spectra and energy levels of Yb+3 in AlN, Applied Physics Letters. 76, 861 (2000).

17. J. F. Philipps, T. Topfer, H. E. Heidepriem, D. Ehrt and R. Sauerbrey, Spectroscopic and lasing properties of Er^{+3} and Yb^{+3} doped fluoride phosphate gasses. Applied Physics B 72. 399-405 (2001).

18. B. Monemar, Lumincescense in III-nitrides, Material Sciences and Engineering, B59, 122 (1999).

19. D. Dexter, Theory of sensitized luminescence in solids. Journal of Chemical Physics 21 836 (1953).

20. M. Maqbool, H. H. Richardson, and M. E. Kordesch. Luminescence from praseodymium doped AlN thin films deposited by RF magnetron sputtering and effect of material structure and thermal annealing on the luminescence, Journal of Material Science 42, 5657-5660 (2007).

21. L.C. Cho and A.J. Steckl, Room-temperature visible and infrared photoluminescence from Pr-implanted GaN films by focused-ion-beam direct write, Appl. Phys. Lett. 74, 2364-2366 (1999).

22. Michael E. Levinshtien, S. L. Rumyantsev and M. S. Shur. Properties of Advances Semiconductor Materials, John Wiley and Sons, Inc. 2001.

23. M. L. Caldwell, A. L. Martin, V. I. Dimitrova, P. G. Van Patten, M. E. Kordesch and H. H. Richardson. Emisson properties of amorphous AlN: Cr^{+3} thin film phosphor. Applied Physics Letters 78, 1246 (2001).

24. S. C. Jain, III-nitrides: growth, characterization, and properties. M. Willander, J. Narayan, R. Van Overstraeten, Journal of Applied Physics 87, 965 (2000).

25. Benjamin Mills, http://www.benjamin-mills.com/chemistry/structures/

26. H. J. Lozykowski, W. M. Jadwisienczak, I. Brown. Photoluminescence and cathodeluminescence of GaN dope with Pr. Journal of Applied Physics 88, 210 (2000).

27. (ACS) http://portal.acs.org/portal/acs/corg/content

28. Taylor, John R. An Introduction to Error Analysis: The Study of Uncertainties in Physical Measurements. University Science Books, 1982.

29. N. Arora, D. Martins, D. Ruggerio, E. Tousimis, A. J. Swistel, M. P. Osborne, R. M. Simmons, Effectiveness of a noninvasive digital infrared thermal imaging system in the detection of breast cancer, The American Journal of Surgery 196, 523-526 (2008).